Journal of Magnetism and Magnetic Materials 485 (2019) 69–74

Contents lists available at ScienceDirect

Journal of Magnetism and Magnetic Materials

journal homepage: www.elsevier.com/locate/jmmm

Research articles

Edge effects on Dzyaloshinskii domain wall tilting

Maokang Shen, Yue Zhang*, Wei Luo, Long You, Xiaofei Yang

School of Optical and Electronic Information, Huazhong University of Science and Technology, Wuhan 430074, PR China

ABSTRACT

Interfacial Dzyaloshinskii-Moriya interaction (DMI) of a heavy metal (HM)/ferromagnetic (FM) metal heterostructure is vital to the current-induced fast domain wall motion. The tilting of the moving Dzyaloshinskii domian wall (DW) has been paid much attention. In this work, using the micromagnetic simulation, we find the DW tilting is originated from different initial DW velocity at two edges because of the initial *antisymmetric* magnetic structure at two edges. In the very early stage of DW motion, the DMI energy traps the DW motion at one edge. For a track whose width is smaller than a critical value, the edge effect plays a major role for DW tilting. This modifies the track width dependence of tilting angle and relaxation time derived from the collective coordinate method without considering edge effect. When the track is wide enough, a temporary vortex-like moment structure inside DW and variation of DW chirality at the edge appear in the process of generating DW tilting for reducing DMI and demagnetization energy.

Current-induced-domain-wall-motion (CIDWM) has potential for developing novel magnetic logic and memory devices with low dissipation [1]. In last decade, current assisted magnetization reversal and domain wall (DW) motion in heavy metal (HM)/ferromagnetic (FM) layered structures with interface spin-orbit coupling and perpendicular magnetic anisotropy (PMA) has attracted much interest due to the low critical current density and high DW velocity [2–6]. The fast DW motion is relevant to an antisymmetric exchange coupling, Dzyaloshinskii-Moriya interaction (DMI), at the HM/FM interface [6,7]. The tilting of DW with strong DMI has been observed under a magnetic field or spin-orbit torque (SOT) [8–10]. This DW tilting is bad for increasing the storage density of memory devices [11].

Boulle et al. depict the DW tilting using the collective coordinate method (CCM) with the tilting angle as an added collective coordinate, and the DMI-related DW tilting is ascribed to the tradeoff among DMI, SOT, and shape anisotropy energy of DW [9]. The evolution of DW tilting is determined by solving the Thiele equations including the central position q, the azimuthal angle φ of the moment in the central DW, and the tilting angle β for the DW plane [9,10]. However, the edge effect is not considered in the traditional CCM (Fig. 1(b)-(d)). This offers the *same initial conditions* for solving the Thiele equations. Therefore, the CCM is inadequate to reveal the difference of CIDWM between the inside track and at the boundary.

Considering the edge energy, Muratov et al. prove the energy stability for a straight tilting DW plane under an external magnetic field when DMI is strong enough [12]. In experiment, Kim et al. find that the DW tilting is governed by the speed asymmetry due to different effective fields at two boundaries [13]. The prerequisite for generating such distinct effective fields at two boundaries is bending the DW plane by an out-of-plane magnetic field. However, this precondition is not necessary for the SOT-induced DW tiling with strong DMI [8,9].

In addition to edge effect, the size and shape of the medium also matters. Garg et al. observe the chirality-independent DW tilting in a curved track [14]. In a circular dot, Baumgartner et al. notice that the evolution of DW tilting lasts so long (>1 ns) that the direction of DW tilting even depends on the mode (static or time-resolved) of observation [15,16]. It is noticed that the medium size in the experimental investigations is on micrometer scale, which is much larger than that in the CCM study (around 100 nm) [9]. The mechanism for DW tilting in a narrow track can be quite different from that in a wide one.

In a word, the mechanism for the DMI-related DW tilting is still not quite clear. Especially, how the DW tilting evolves on different *size* scale from a *microscopic dynamical* perspective is still an open question. In this work, using micromagnetic calculation, the evolution of DW tilting is studied from a microscopic perspective. Without considering extrinsic factors such as defects, the DW tilting is originated from the *antisymmetric* moment structure at two track boundaries. This leads to different initial velocities of the local DW at two boundaries. After the antisymmetry breaking, the DW tilts in different processes that depend on track width (w).

The SOT-induced DW motion was simulated by the software named the Object-Oriented MicroMagnetic Framework (OOMMF) containing the codes of damping-like SOT and DMI [17]. We considered the CIDWM in a 50–400-nm-wide, 1000–2000-nm-long, and 0.6-nm-thick track. The dimension of unit cell was 1 nm (length) × 1 nm (width) × 0.6 nm (thickness). The parameters of Co/Pt, a typical ultrathin film with PMA and strong DMI, were used [11,18]: the saturation magnetization $M_S = 7 \times 10^5$ A/m, the PMA constant $K = 8 \times 10^5$ J/

* Corresponding author.
E-mail address: yue-zhang@hust.edu.cn (Y. Zhang).

https://doi.org/10.1016/j.jmmm.2019.04.063
Received 19 January 2019; Received in revised form 29 March 2019; Accepted 16 April 2019
Available online 17 April 2019

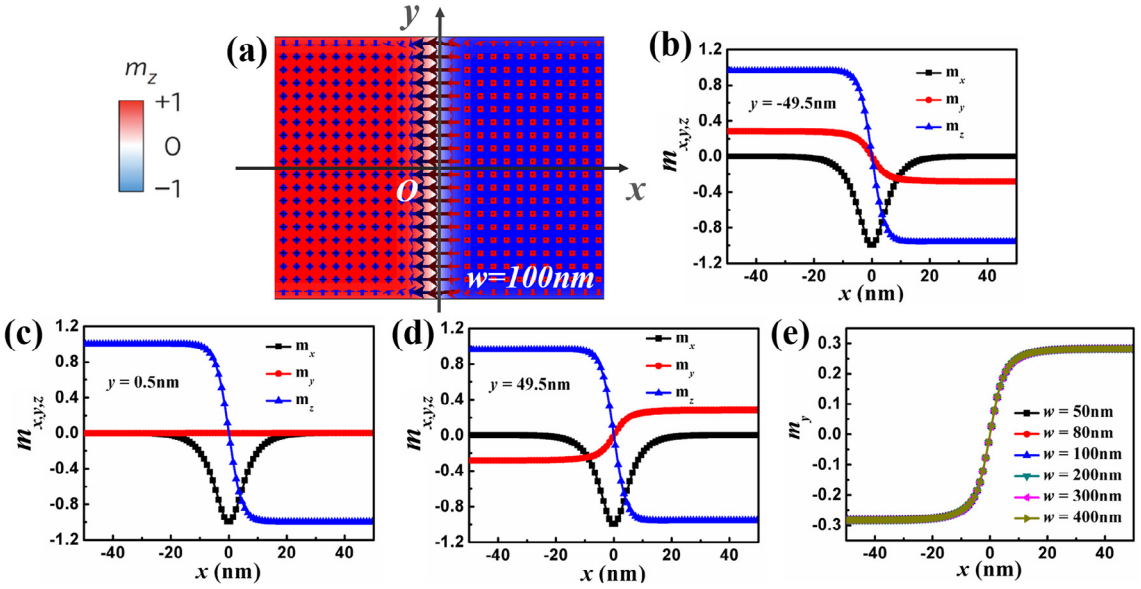

Fig. 1. Moment structure of the left-handed Néel-typed DW (a), the variation of m_x, m_y, and m_z (normalized vector for the orientation of moment) across the DW region at the lower boundary (b), in the inner part (c), and at the upper boundary of the track (d); the variation of m_y across the DW region at the upper boundary of the tracks with different w (e).

m^3, the exchange stiffness constant $A = 1 \times 10^{11}$ J/m, the DMI constant $D = -1.5$ mJ/m^2, the current density $J = 5 \times 10^{11}$ A/m^2, the spin Hall angle $\theta_{SH} = 0.08$, and the damping coefficient $\alpha = 0.03$. The α is smaller than the real value [19] for prolonging the relaxation in order to reveal the early evolution of DW tilting in detail. In general, the current gives rise to an Oersted field at the track edge [20]. Based on the composition and shape of the track, we have simulated the current-induced Oersted field using the COMSOL-Multiphysics software. We find the Oersted field concentrated near the two track edges is not higher than 20 Oe. The OOMMF simulation indicates that such a weak edge field makes a negligible impact on the dynamics of DW tilting (See more details in the section S1 of the Supplementary Materials).

Initially, a stable DW was generated in the middle of the track. Because of the negative D, the DW exhibits a Néel-typed structure with left-handed chirality (Fig. 1(a)). Inner the track (Fig. 1(c)), the moments rotate in the xz plane across the DW region. Near the two boundaries, however, the moment has a small projection on the y axis due to the DMI-related boundary condition [17]. The direction for the moment projection at one boundary is opposite to that at the other one, resulting in the antisymmetric moment structure (Fig. 1(b) and (d)). The increase of w from 50 nm to 400 nm makes little impact on the moment structure at the boundary (Fig. 1(e)).

We found the early evolution of q and φ inside the track and at the boundary is quite different. At the lower boundary, the local DW moves clearly faster than the upper one (Fig. 2(a) and (d)), which is accompanied with a faster rotation of the moment in the middle of the DW at the lower boundary (Fig. 2(b) and (e)). The tilting angle of the DW plane becomes constant after the DW velocities and the boundary azimuthal angles become stable (Fig. 2(c) and (f)). The w also influences the evolution of q, φ, and β. When w is 400 nm, a peak of φ appears at around 0.2 ns (Fig. 2(e)). The relaxation time (τ) for reaching the final stable state increases with w. The β also increases with w but becomes almost constant when w is 200 nm or larger (Fig. 2(g)). In Ref. 9, Boulle et al. derive a w-independent β without limitation on the range of w. On the other hand, Boulle et al. suggest the τ against w appears to have a quadratic relationship for a wide track. In this work, this quadratic function is satisfied only when $w \geq 200$ nm (Fig. 2(h)). When the w is in the range between 50 nm and 400 nm, a cube relaxation seems more suitable for fitting the τ as a function of w, and a turning point appears around $w = 200$ nm (Fig. 2(i)). This hints the mechanism for the relaxation of DW tilting depends on w.

To ascertain the detailed process of DW motion at the boundary, the evolution of the moment structure at the boundary was collected (Fig. 3). One can see that the initial antisymmetric moment structure ($t = 0$ ns) is destroyed in the early stage of CIDWM. When $t = 0.1$ ns, the moments in the central DW at the lower boundary are rotated easily, resulting in a sharp transition of moment orientation across the local DW. However, at the upper boundary, the variation of moment orientation across the local DW is very smooth at 0.1 ns and 0.2 ns. This evolution of moment structure at the boundary within the first 0.2 ns does not depend on w. However, the increase in w prolongs the relaxation and changes the DW structure at the lower boundary temporally (Fig. 3(c) and (e)). In the tracks with $w = 200$ nm and 400 nm, when $t = 0.1$ ns, the moment at the lower boundary rotates anticlockwise from left to right but it changes to be clockwise afterwards. This temporal reversing of chirality lasts longer in a wider track.

In addition to the moment of DW at the boundary, the evolution of moment structure inside the DW is also related with w (Fig. 4). In the tracks for all w, the SOT-induced moment rotation nucleates at the lower boundary when $t = 0.1$ ns (Fig. 4(a), (e), and (i)). This is width-independent and breaks the initial antisymmetric moment structure at two boundaries. Afterwards, the area for the moment rotation expands towards the upper boundary till the moment distribution becomes homogeneous again. To see more details, the minimum of m_y ($(m_y)_{min}$) across the track width direction is shown in Fig. 4(d), (h), and (l). There is only one valley of $(m_y)_{min}$ across the track width direction during the DW tilting for $w = 100$ nm. When w increases to 200 nm or 400 nm, the tilting of DW is accompanied with the appearance of more valleys of $(m_y)_{min}$ (Fig. 4(f), (j), (h), and (l)) (The DW motion for $w = 400$ nm is also exhibited in Movie 1 in the Supplementary materials).

The evolution of moment structure of DW shown in Figs. 3 and 4 reveals the microscopic mechanism for DW tilting in different w ranges (Fig. 2(g)). When w is 200 nm or higher, edge effect plays a negligible role, which gives rise to the w-independent β and the τ as a quadratic function of w. This is consistent well with the prediction by Boulle et al. [9]. Nevertheless, for the narrower track, the edge effect (a size effect on the nanometer scale) cannot be neglected, which modifies the w dependence of β and τ. Deep quantitative analysis for this edge-relevant β and τ seems rather tedious in mathematics. However, the quantitative analysis based on free energy may offer insight for understanding the

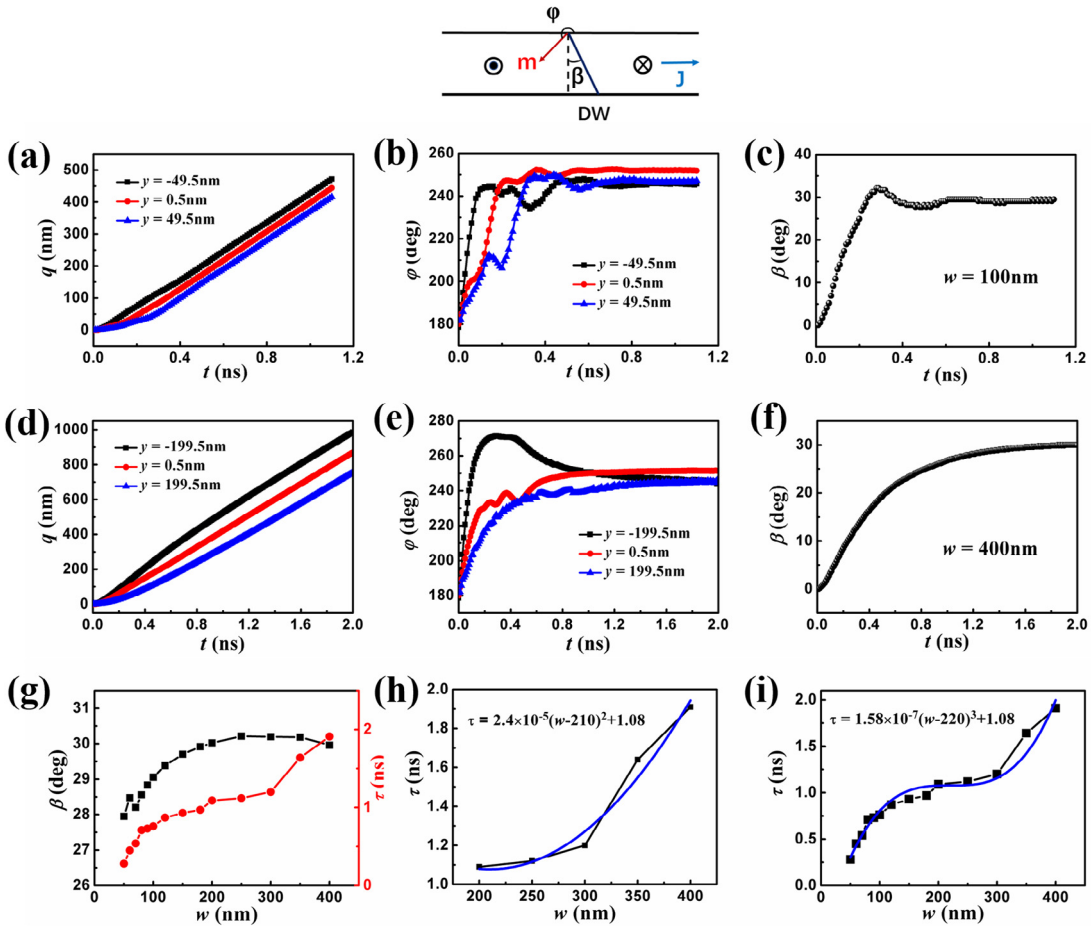

Fig. 2. Time-dependence of q, φ, and β of the DWs at the two boundaries and in the inner track with the w of 100 nm ((a)-(c)) and 400 nm ((d)-(f)); β and relaxation time (τ) as a function of w (g); the fitted relaxation time as a function of w using the power law with w varying between 200 nm and 400 nm (h) and between 50 nm and 400 nm (i). The solid blue lines are the fitting curves.

physical mechanism for the edge effect on DW tilting.

The DW velocity at the boundary is relevant to edge energy. According to the Landau-Lifshitz-Gilbert equation, the speed for the dynamics of moment is proportional to the effective field that is derived from free energy. Therefore, a strong edge energy favors a fast relaxation of the moment at the boundary. Based on the moment structure shown in Fig. 3, the edge free energy density including anisotropy energy, demagnetization energy, exchange energy, and the DMI energy at different time were all derived. Except for DMI, the other three energies at two boundaries are quite similar (not shown). When $w = 100$ nm, the DMI energy densities at two boundaries are quite different at 0.1 ns (Fig. 5(a)). At the upper boundary, the lower DMI energy offers a trap that pins the reorientation of moment. When $t = 0.5$ ns, the energy densities at two boundaries become the same, resulting in the same DW velocity. For $w = 400$ nm, the DMI energy keeps increasing at the upper boundary. Nevertheless, it is enhanced drastically at 0.5 ns but reduced at 1.5 ns (Fig. 5(b)).

The different mechanism for DW tilting for different w can also be seen from the evolution of the total energy at two track boundaries (Fig. 5(c) and (d)). For $w = 100$ nm, the boundary energies at two boundaries vary abruptly at different time. At the lower boundary, the abrupt change of energy happens immediately after the current is applied. However, at the upper one, it delays for about 0.2 ns. As to $w = 400$ nm, the upper boundary energy increases gradually. At the lower boundary, however, a maximum energy appears at around 0.3 ns. Afterwards, this lower boundary energy is reduced gradually till it becomes identical to that at the upper one.

In addition to edge energy, the energies of the whole track including demagnetization, exchange, DMI, and anisotropy were also derived (Fig. 6). When the track is 100 nm wide, the DMI, exchange, and anisotropy energies increase but the demagnetization energy decreases in the process of generating the DW tilting. All the energies vary in the first 0.3 ns during which time the moment rotation nucleates at the lower boundary and expands towards the upper one. For the 400-nm-wide track, the exchange energy keeps increasing and the demagnetization energy keeps decreasing in the first 1 ns. On the other hand, the DMI reaches a maximum value at around 0.3 ns. When the track is very wide, the expansion of a single area for moment rotation seems not favorable in energy, and the reproduction of nucleus reduces DMI and demagnetization energy at the cost of increasing exchange energy.

The energy analysis for the whole track hints the reason for the w dependence of DW tilting. There is a critical size for the area of moment rotation for the requirement of lowering energy (Figs. 4 and 6). When w is smaller than this critical size, edge effect is not negligible, and the DW tilting becomes related to w. On the other hand, when the track is wider than this critical size, the reproduction of nucleus inside the DW decides the DW tilting. Since most moments contributing to the DW tilting are far away from the edge, the intrinsic parameters of magnetic system determine their dynamical progress and the final stable moment structure in DW. Therefore, the tilting angle is irrelevant to w.

Based on the simulation results, the progress of DW tilting can be understood as following. In our condition, the current flowing in the x direction offers the damping-like SOT that rotates the moments towards $-y$ direction. Afterwards, the moments are switched to the z direction by the DMI torque [7]. This process is equal to moving the DW to the right. (The direction for DW motion and tilting is reversed when the

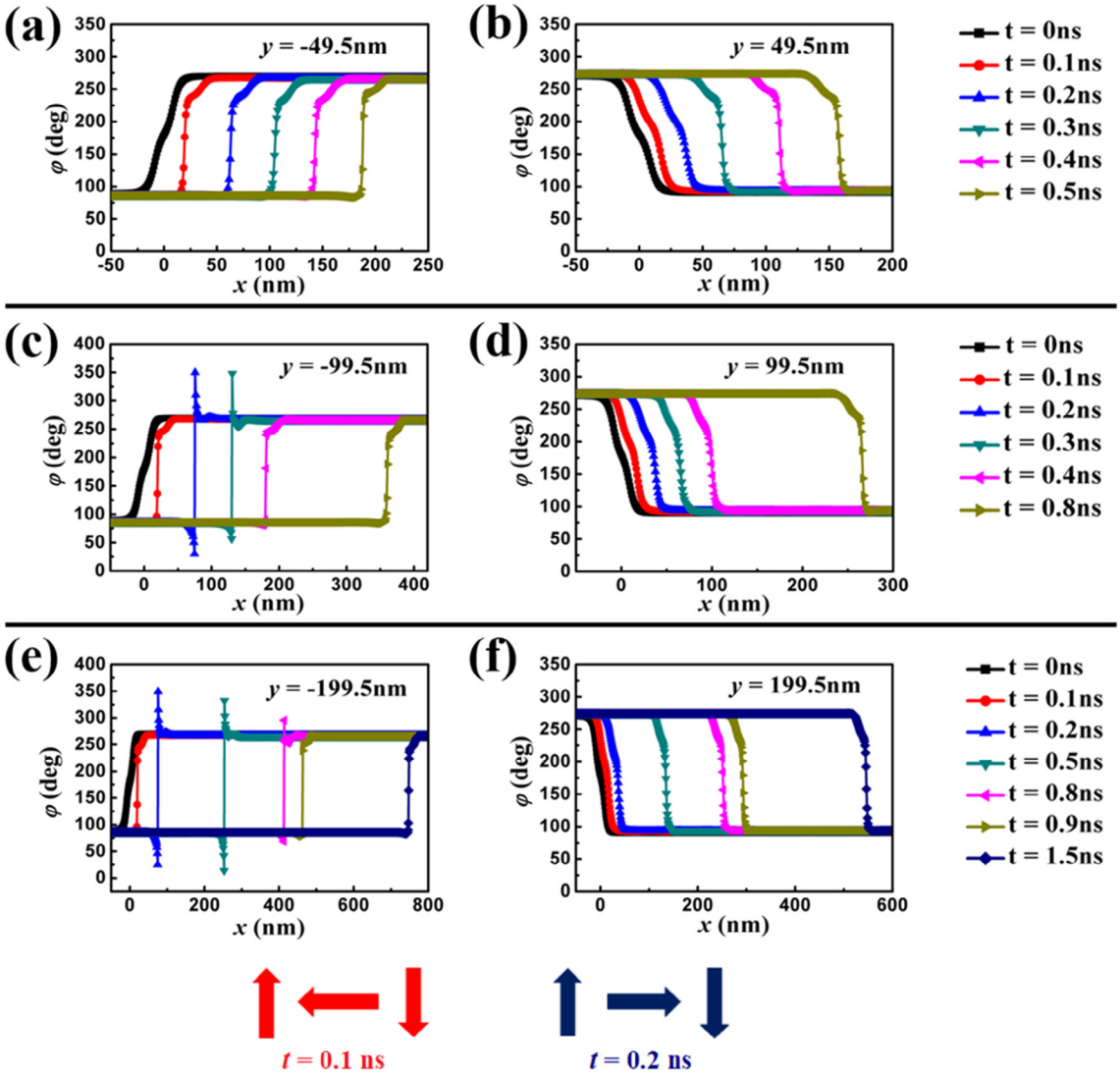

Fig. 3. Evolution of the spatial distribution of φ across the DW at the lower ((a), (c), and (e)) and upper ((b), (d), and (f)) boundary of the track with different w in the early stage of the CIDWM. The moment structure at the lower boundary at different time for w = 200 or 400 nm is shown below.

current direction is reversed (Fig. 2 in the Supplementary Materials)). Therefore, in the early stage of DW motion, what determines the initial DW velocity is not the moment orientation in the central but that at the right side of DW. According to the boundary moment structure (Fig. 1(a)), the moments at the right side of DW plane at the lower boundary are easy to be rotated to the – y direction by SOT in a very short time, which results in the enhanced DMI energy and the high velocity. On the contrary, at the right side of DW plane at the upper boundary, the moment rotation towards the – y direction needs to escape the DMI energy trap when the moments are rotated to the – x direction. As a result, the early DW motion at the upper boundary is pinned, and this difference in the initial velocity for the upper and lower DW moments is independent on w (Fig. 3). Nevertheless, the following process depends on w. When w is 100 nm or smaller, the upper moments cannot escape the DMI energy trap until the moment rotation transfers to the upper boundary (Figs. 4(a)-(d), and 5(c)). On the other hand, when w is 200 nm or larger, the DW tilting is realized by the continuous reproduction of nucleus inside DW (Fig. 4(f), (h), (j), and (l)). This changes the chirality of the moment structure of the DW at the lower boundary and prolongs the relaxation. Finally, no matter what w is, the DW structure at two boundaries become antisymmetric again, and the DW velocities at the two boundaries become the same, leading to the final stable DW tilting with a constant β.

The microscopic dynamical process revealed by the micromagnetic simulation is not easy to study experimentally or theoretically. In experiment, one needs to observe the evolution of moments in a very small region in a very short duration (< < 1 ns). In CCM, the dynamics of DW can be depicted by several collective coordinates based on the assumption of a *homogenous* moment distribution in DW. Therefore, the CCM may not depict the SOT-induced motion of the DW with *strong* DMI precisely, since it ignores the edge effect that leads to the inhomogeneous moment structure during the evolution of DW tilting, especially for a narrow track. In the experimental observation about DW tilting, the w is usually tens of micrometers, and the medium morphology and the pinning due to edge defects may also influence the DW tilting [13,15,16]. In this case, the CCM seems too simple to reveal the mechanism for DW tilting.

In summary, to understand the mechanism for the tilting of DW with strong DMI in CIDWM, the DMI-related antisymmetric moment structure at the two boundaries needs to be considered. This antisymmetry is destroyed in the early stage of the unidirectional CIDWM. For a left-handed DW moving to the right, the moments at the right side of DW at the lower boundary are easy to rotate, resulting in a higher initial velocity. At the upper one, the moment rotation at the right side of DW needs to escape the energy traps of DMI, leading to a lower initial velocity. On the other hand, when the track is wide enough, the moment

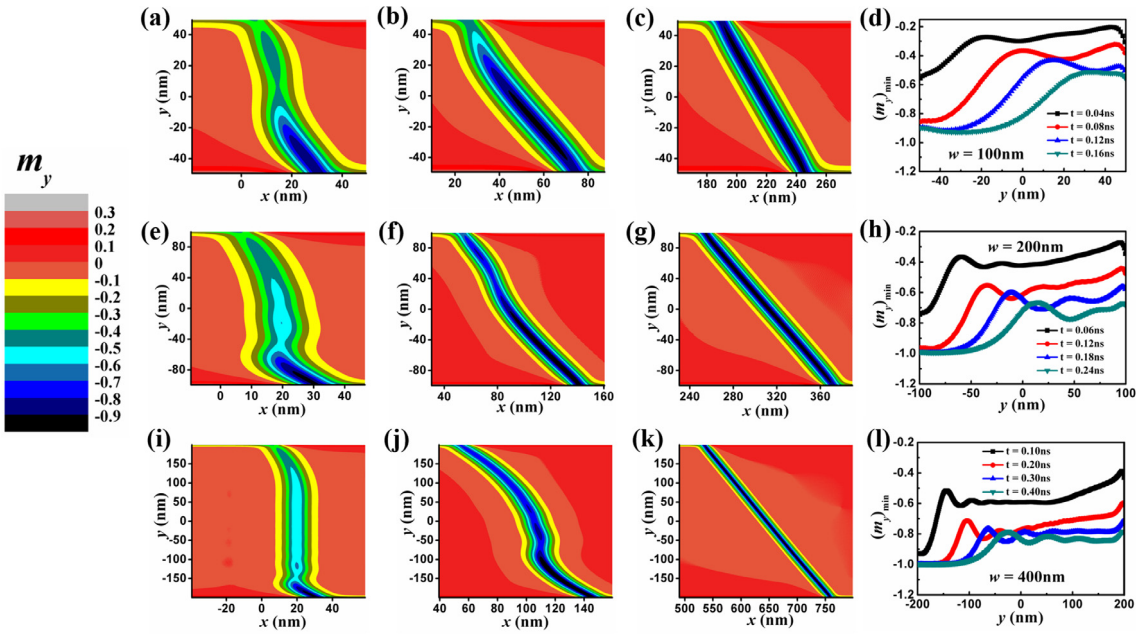

Fig. 4. Spatial distribution of m_y in the DW of the track with different w and at different time (t = 0.1 ns (a), 0.2 ns (b), and 0.6 ns (c) for w = 100 nm; t = 0.1 ns (e), 0.3 ns (f), and 0.8 ns (g) for w = 200 nm; t = 0.1 ns (i), 0.3 ns (j), and 1.5 ns (k) for w = 400 nm); the minimum of m_y ($(m_y)_{min}$) as a function of y across the track width direction for w = 100 nm (d), 200 nm (h), and 400 nm (l).

structure of DW is significantly changed during the evolution of DW tilting for reducing DMI and demagnetization energies, resulting in the temporary reversed moment chirality at one boundary. This enhances the DMI energy at the edge and prolongs the relaxation process of DW tilting. Finally, the moment structure of DW at two boundaries recovers to antisymmetry and the DW tilting becomes stable finally.

Acknowledgements

This work was supported by the National Natural Science Foundation of China [grant number 11574096] and Huazhong University of Science and Technology (No. 2017KFYXJJ037).

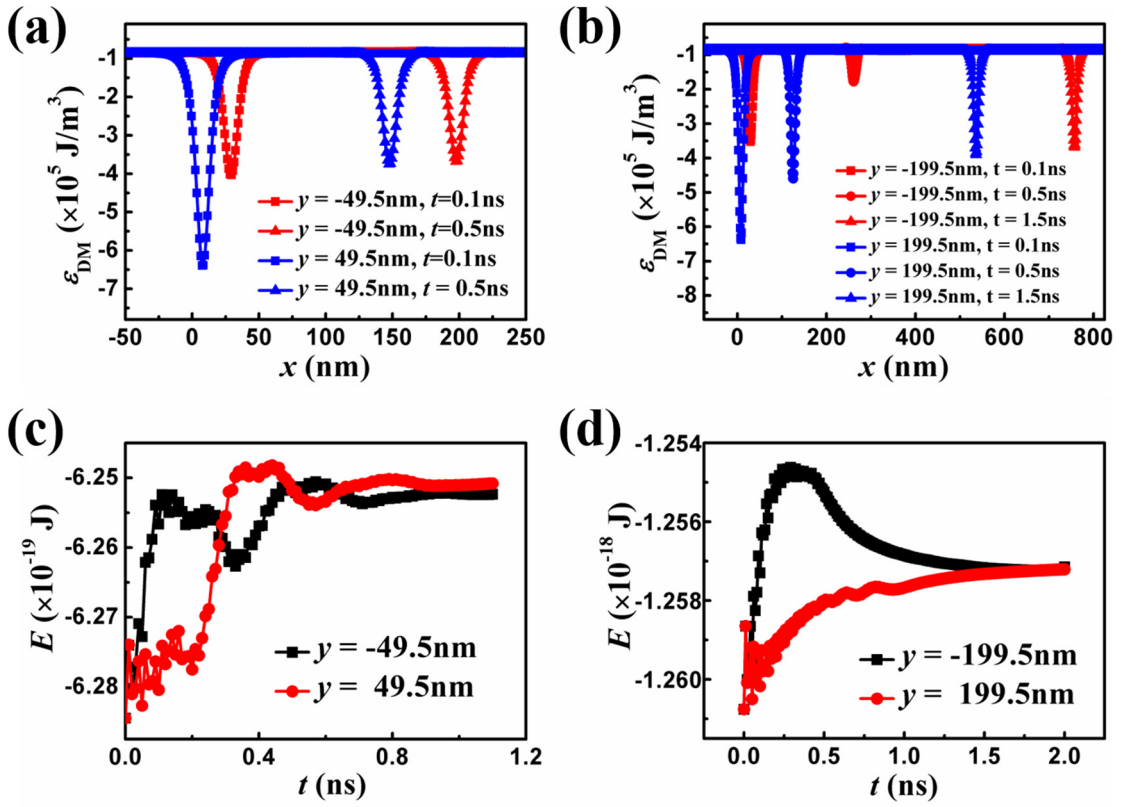

Fig. 5. Energy densities of DMI at different time ((a) and (b)) and the evolution of total energy ((c) and (d)) at the upper and lower boundaries in the track with different w.

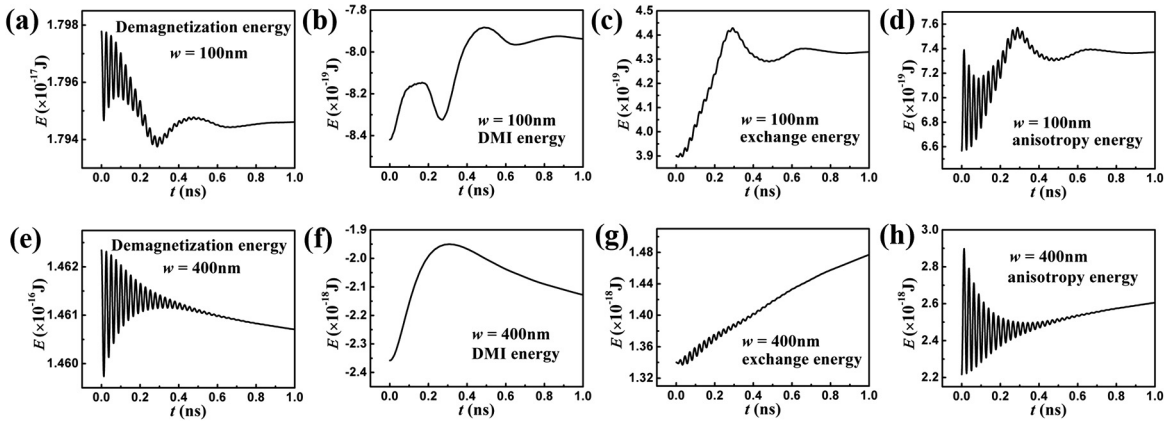

Fig. 6. Energies of demagnetization, DMI, exchange, and anisotropy for the 100-nm-wide track ((a)–(d)) and the 400-nm-wide track ((e)–(h)).

Appendix A. Supplementary data

Supplementary data to this article can be found online at https://doi.org/10.1016/j.jmmm.2019.04.063.

References

[1] S.S.P. Parkin, M. Hayashi, L. Thomas, Science 320 (2008) 190.
[2] W.W. Lin, H. Sang, D. Liu, Z.S. Jiang, A. Hu, X.S. Wu, G. Xiao, J. Appl. Phys. 99 (2006) 08G518.
[3] K.X. Xie, W.W. Lin, H.C. Sun, Y. Nie, H. Sang, J. Appl. Phys. 104 (2008).
[4] P.P.J. Haazen, E. Murè, J.H. Franken, R. Lavrijsen, H.J.M. Swagten, B. Koopmans, Nat. Mater. 12 (2013) 299.
[5] K.-S. Ryu, L. Thomas, S.-H. Yang, S. Parkin, Nat. Nanotech. 8 (2013) 527.
[6] S. Emori, U. Bauer, S.-M. Ahn, E. Martinez, G.S.D. Beach, Nat. Mater. 12 (2013) 611.
[7] S.-H. Yang, S. Parkin, J. Phys.: Condens. Matter 29 (2017).
[8] K.-S. Ryu, L. Thomas, S.-H. Yang, S.S.P. Parkin, Appl. Phys. Express 5 (2012).
[9] O. Boulle, S. Rohart, L.D. Buda-Prejbeanu, E. Jué, I.M. Miron, S. Pizzini, J. Vogel, G. Gaudin, A. Thiaville, Phys. Rev. Lett. 111 (2013).
[10] E. Martinez, S. Emori, N. Perez, L. Torres, G.S.D. Beach, J. Appl. Phys. 115 (2014).
[11] M. Shen, Y. Zhang, L. You, X. Yang, Appl. Phys. Lett. 113 (2018).
[12] C.B. Muratov, V.V. Slastikov, A.G. Kolesnikov, O.A. Tretiakov, Phys. Rev. B 96 (2017).
[13] D.-Y. Kim, M.-H. Park, Y.-K. Park, J.-S. Kim, Y.-S. Nam, H.-S. Hwang, D.-H. Kim, S.-G. Je, B.-C. Min, S.-B. Choe, Phys. L Rev. B 97 (2018).
[14] C. Garg, S.-H. Yang, T. Phung, A. Pushp, S.S.P. Parkin, Sci. Adv. 3 (2017).
[15] M. Baumgartner, K. Garello, J. Mendil, C.O. Avci, E. Grimaldi, C. Murer, J. Feng, M. Gabureac, C. Stamm, Y. Acremann, S. Finizio, S. Wintz, J. Raabe, P. Gambardella, Nat. Nanotech. 12 (2017) 980.
[16] M. Baumgartner, P. Gambardella, Appl. Phys. Lett. 113 (2018).
[17] S. Rohart, A. Thiaville, Phys. Rev. B 88 (2013).
[18] X. Zhang, Y. Zhou, M. Ezawa, Nat. Commun. 7 (2016) 10293.
[19] A.J. Schellekens, L. Deen, D. Wang, J.T. Kohlhepp, H.J.M. Swagten, B. Koopmans, Appl. Phys. Lett. 102 (2013).
[20] D. Li, B. Cui, J. Yun, M. Chen, X. Guo, K. Wu, X. Zhang, Y. Wang, J. Mao, Y. Zuo, J. Wang, L. Xi, Nanoscale Res. Lett. 13 (2018) 238.